

Transfer function approximation of motion-induced aerodynamic forces with rational functions

Arno Kirch* and Udo Peil

*Institute of Steel Structures, Technische Universität Carolo-Wilhelmina zu Braunschweig,
Beethovenstraße 51, 38106 Braunschweig, Germany*

(Received May 26, 2010, Accepted September 9, 2010)

Abstract. For a detailed investigation of the dynamic behaviour of slender bridges under wind action especially the motion-induced fluid forces should be available not only for harmonic motions but also for more general ones. If linear transfer behaviour is assumed, the force-displacement relation for almost arbitrary motions can be handled in the frequency domain using aerodynamic transfer functions. In aerospace engineering as well as in bridge engineering, these functions are usually approximated by special kinds of complex-valued rational functions which depend on complex frequencies. The quality of this approximation is evaluated for several bridge cross sections in this article. It is shown that rational functions are for some sections scarcely suitable to realistically represent the transfer behaviour of motion-induced aerodynamic forces for arbitrarily complex frequencies.

Keywords: bridges; rational function approximation; state-space model; flutter; divergence.

1. Introduction

Modern bridges can be built as very slender structures especially when new materials and innovative construction methods are applied. This trend is accompanied by an increased susceptibility to oscillations. The design of extremely slender bridges, such as large-span road or filigree pedestrian bridges, is therefore decisively influenced by their vibration behaviour. Special attention has to be given to wind-induced vibrations. In recent years, a number of techniques have been investigated to improve the vibration behaviour of bridges under the influence of wind by systematically imposing additional forces with passively or actively controlled actuators like tuned mass dampers, gyroscopes or reaction wheels (e.g., Lin *et al.* 1999, Pourzeynali and Datta 2002, Kirch and Peil 2009).

A realistic and mathematically consistent description of the forces caused by the wind flow around the bridge girder is essential for dimensioning these actuators. Usually, wind action is divided into several types of wind forces. Along with its structural properties, motion-induced aerodynamic forces, which are focussed on in this article, define the dynamic characteristics of the so-called aeroelastic system. Due to the effect of motion-induced aerodynamic forces, aeroelastic instabilities can occur in the form of flutter and aeroelastic divergence if the speed of the wind flow

* Corresponding Author, E-mail: a.kirch@is.tu-braunschweig.de

exceeds critical values. Avoiding aeroelastic instabilities crucially influences the design of very slender bridges. An adequate mathematical description of the motion-induced aerodynamic forces is the precondition for a detailed theoretical analysis of the system behaviour within all wind-speed ranges.

The article is divided into four main sections. Section 2 addresses the mathematical definition and notation of the motion-induced aerodynamic forces. Important terms of system theory are mentioned in this context. In Section 3, the general rational approach for the transfer function and several special cases are introduced. The correspondent functions in the time domain are used to explain the approach in a more understandable way. Section 4 describes the quality of a special kind of rational functions, commonly used in bridge as well as in aerospace engineering for approximating the transfer functions of motion-induced aerodynamic forces. For two cross sections, whose motions cause totally different flows and hence forces, the results are described in detail. Findings for other selected cross sections are presented in table form. Finally, Section 5 explains how approximation quality influences the dynamic model characteristics of an aeroelastic system again using the two cross sections from the previous section.

2. Expressions for motion-induced aerodynamic forces

In civil engineering, motion-induced aerodynamic forces of a two-dimensional system with two aerodynamically effective degrees of freedom are usually defined according to Simiu and Scanlan (1996) as follows

$$\begin{aligned} L &= \frac{1}{2}\rho U^2 B \left(KH_1^* \frac{\dot{h}}{U} + KH_2^* \frac{B\dot{\alpha}}{U} + K^2 H_3^* \alpha + K^2 H_4^* \frac{h}{B} \right) \\ M &= \frac{1}{2}\rho U^2 B^2 \left(KA_1^* \frac{\dot{h}}{U} + KA_2^* \frac{B\dot{\alpha}}{U} + K^2 A_3^* \alpha + K^2 A_4^* \frac{h}{B} \right) \end{aligned} \quad (1)$$

The degrees of freedom h and α are shown in Fig. 1. In the terms outside the brackets of Eq. (1), U symbolises the constant horizontal mean wind speed, ρ stands for the air density and B denotes the total deck width. The dot ($\dot{}$) symbolises the differentiation with respect to time t . As can be seen in Fig. 1, L is the vertical aerodynamic force and M is the resultant aerodynamic moment related to the middle of the deck. The coefficients H_j^* and A_j^* are functions of the reduced frequency

$$K = \omega B / U = 2\omega b / U = 2k \quad (2)$$

of the harmonic oscillation. Whereas the reduced frequency K , often used in bridge engineering, is related to the total deck width B , the reduced frequency k is defined using the half deck width b . Here, the variable k is preferred, as it is usually done for aircraft wings and in many studies of bridges. The coefficients H_j^* and A_j^* can be identified experimentally or numerically (e.g., Starossek *et al.* 2009). For the flat plate, analytical solutions based on the potential theory are available (Theodorsen 1934, Küssner 1936). In this article, the flat-plate case always means the theoretical one unless otherwise noted.

To avoid inconsistencies, the Scanlan notation Eq. (1) is applicable for harmonic oscillations only. Mathematical problems occur for all other kinds of motion because both time-domain and frequency-

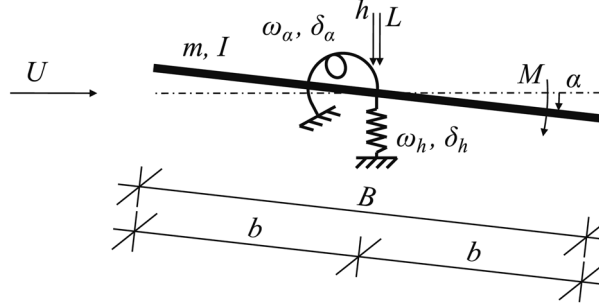


Fig. 1 Two-dimensional aeroelastic system with two aerodynamically effective degrees of freedom

domain information are used. A consistent, pure frequency-domain formula is applied especially in aerospace engineering.

$$\mathbf{f}(p) = \begin{pmatrix} Lb \\ M \end{pmatrix}_{(p)} = \pi \rho b^2 U^2 \cdot \begin{pmatrix} Q_{11} & Q_{12} \\ Q_{21} & Q_{22} \end{pmatrix}_{(p)} \cdot \begin{pmatrix} h/b \\ \alpha \end{pmatrix}_{(p)} = q_0 \cdot \mathbf{Q}(p) \cdot \boldsymbol{\xi}_s(p) \quad (3)$$

This notation is the standard for most investigations on aeroservoelasticity problems of aircrafts and has been used since early publications on aerodynamics (Küssner and Schwarz 1940). In the abbreviated form, the vector \mathbf{f} contains the aerodynamic forces and the vector $\boldsymbol{\xi}_s$ includes the aerodynamically effective degrees of freedom. The frequency-domain variable p stands for the reduced complex frequency

$$p = sb/U = (\sigma + i\omega)b/U = \beta + ik \quad (4)$$

where s denotes the non-reduced complex frequency. The imaginary part of s is the reduced frequency k , already defined in Eq. (2). In this article, the dimensionless coefficients A_j^* and H_j^* as well as the \mathbf{Q} elements are all termed (aerodynamic) derivatives.

A dimensionless \mathbf{Q} matrix is obtained when using identical dimensions for both the different types of deformations and the different types of loads. Without any difficulty, an extension of this notation to additional degrees of freedom, like horizontal displacement or motions of aerodynamically effective control shields (Kirch *et al.* 2009a,b), is possible. When introducing a harmonic approach in the Scanlan formula, the Eqs. (1) and (3) can be directly compared for imaginary frequencies $p = 0 + ik$.

$$Q(ik) = \frac{k^2}{\pi} \begin{pmatrix} 2(H_4^*(ik) + iH_1^*(ik)) & 4(H_3^*(ik) + iH_2^*(ik)) \\ 4(A_4^*(ik) + iA_1^*(ik)) & 8(A_3^*(ik) + iA_2^*(ik)) \end{pmatrix} \quad (5)$$

The notation of the matrix elements in the right part of Eq. (5) or similar ones (Theodorsen and Garrick 1941, Klöppel and Thiele 1967) have several disadvantages compared with the elements of the \mathbf{Q} matrix. Since the reduced frequency k is separated, they cannot be seen as independent frequency-domain functions. This can lead to several mathematical problems and inconsistencies. A detailed discussion of these problems is not part of this article.

When regarding its variables as unilateral Laplace transforms, Eq. (3) is the frequency domain representation of a linear time-invariant transfer element, which is usually described as follows

$$\mathbf{f}(p) = \mathbf{G}(p) \cdot \xi_s(p) \quad (6)$$

Forces result as a product of the aerodynamic transfer function \mathbf{G} and the displacements ξ_s . In this article, the aerodynamic transfer function is alternatively termed aerodynamic admittance. Apart from q_0 , the transfer function of motion-induced aerodynamic forces basically consists of the derivative matrix \mathbf{Q} .

Usually, analytic functions of the complex frequency are taken to express the transfer function. With these functions, the derivatives of bridge cross sections, which are available in most cases only for harmonic oscillations, are approximated. Harmonic oscillations are described by complex-conjugate frequencies on the imaginary axis. Hence, the identification is only done along the imaginary axis. Additionally, the original values of the aerodynamic derivatives are only determined for discrete frequencies within a finite interval. It is thus questionable whether the approximation can be used to realistically model the aerodynamic transfer behaviour for complex frequencies with an arbitrary location in the complex frequency plane.

In Jones (1938) and Garrick (1938), first proposals for approximation functions were made in terms of step responses in the time domain. Rational transfer functions can be regarded as a generalisation of Jones' approach. Further examples of analytical transfer function approximations are Stark's approach (Stark 1984), which can be considered as a generalisation of Garrick's approach, or fractions of sums of Chebyshev polynomials - that means special rational functions - which are applied in Botez *et al.* (2007).

Similar to Eq. (3) or Eq. (6), gust-induced forces, which constitute another type of wind forces, can be connected with mean-value-free, fluctuating velocity components of gusts by corresponding transfer functions. Gust-induced forces will be only marginally mentioned in this article.

3. Rational function approaches for the aerodynamic transfer function

Rational functions are the most commonly used analytical expressions for approximating the aerodynamic transfer behaviour in aerospace as well as in bridge engineering. A complex partial fraction expansion of this transfer approach is most suitable for an investigation. For one element of the derivative matrix the approximation function is as follows

$$Q(p) = A_0 + A_1 p + A_2 p^2 + \sum_{\mu=1}^n \sum_{\kappa=1}^{v_{\mu}} \frac{A_{\mu\kappa}}{(p + \gamma_{\mu})^{\kappa}} \quad (7)$$

The poles of the transfer function are denoted by $(-\gamma_{\mu})$ and their order or multiplicity by v_{μ} . For the sake of clarity, matrix indices of the derivative Q have been omitted. The polynomial part is necessary to approximate at least the theoretical flat-plate derivatives in a reasonable way as will be addressed in Section 4. Due to the linear and the quadratic summand of this part, a non-causality in the transfer behaviour occurs. It disappears, when the equation of motion of the aeroelastic system is assembled.

The rational summands become more comprehensible when examining the impulse response $G(t) = q_0 \cdot Q(t)$ which is an element of the corresponding matrix $\mathbf{G}(t)$, the time-domain analogon of the transfer function $\mathbf{G}(s)$. For all functions that are used in this article, it is assumed that their values are zero prior to $t = 0$. Considering Eq. (7) as a result of a unilateral Laplace transform with the reduced transform variable p , tables of Laplace transforms can be used to determine $Q(\bar{t})$

$$Q(\bar{t}) = A_0 \bar{\delta}(\bar{t}) + A_1 \bar{D}(\bar{\delta}(\bar{t})) + A_2 \bar{D}^2(\bar{\delta}(\bar{t})) + \sum_{\mu=1}^n \sum_{\kappa=1}^{\nu_\mu} A_{\mu\kappa} \frac{\bar{t}^{\kappa-1}}{(\kappa-1)!} e^{-\gamma_\mu \bar{t}} \quad (8)$$

The non-dimensionalised time and the associated dirac impulse are defined as follows

$$\bar{t} = \frac{U}{b} t, \quad \int_{-\infty}^{\infty} \bar{\delta}(\bar{t}) d\bar{t} = 1 \quad (9)$$

The operator \bar{D} symbolises the generalised differentiation with respect to \bar{t} . Since only the rational summands appear for $\bar{t} > 0$, they are also called lag terms.

Regarding the location of their poles ($-\gamma_\mu$), the partial fractions can be separated into several types. The mandatory pole location in the left complex half-plane ensures impulse responses that decrease with time. Usually, simple, real poles ($\nu_\mu = 1, (-\gamma_\mu) \in \mathbb{R}^-$) with real coefficients $A_{\mu\kappa}$ are applied. As a result, the associated impulse responses are decaying exponential functions. Pairs of simple complex-conjugate poles with complex-conjugate coefficients are, however, possible as well. Complex conjugates are necessary to ensure real impulse responses in the time domain which, concerning their partial fractions, can be calculated as

$$A_{\mu\kappa} e^{-\gamma_\mu \bar{t}} + A_{\mu\kappa}^c e^{-\gamma_\mu^c \bar{t}} = |A_{\mu\kappa}| e^{-\text{Re}(\gamma_\mu) \bar{t}} 2 \cos(\text{Im}(\gamma_\mu) \bar{t} - \varphi_{\mu\kappa}) \quad (10)$$

The superscript ()^c indicates the complex-conjugate value and $\varphi_{\mu\kappa}$ the argument of the complex coefficient $A_{\mu\kappa}$. According to Eq. (10), the impulse responses can be considered as decaying cosine functions. In bridge engineering, a similar approach has been used for instance in Sternberg (1992). A systematic investigation of the suitability of complex-conjugate poles for rational aerodynamic transfer functions still needs to be done.

The poles described so far can also be multiple ($\nu_\mu > 1$). For this case, the impulse responses include an additional factor in the form of $\bar{t}^{\kappa-1}/(\kappa-1)!$ which is dominant for small time values. The proposal to use multiple real poles was published in Eversman and Tewari (1991) and is in their article recommended for derivatives of airfoils at high Mach numbers. Own investigations, which have not been published so far, have shown that the application of multiple real poles is appropriate for approximating the theoretical gust admittance of the flat plate.

Concerning the constant summand of the polynomial part and clever combinations of the rational summands of Eq. (7), it could be an interesting task to find more or less realistic, parallel connected mechanical systems that possess a similar transfer behaviour. This is attempted in Omenzetter et al. (2000) for a simple real pole. Certainly, this kind of analogy would help users to understand the rational approach in a better way.

Using simple real poles which are the same for all derivatives is most common in aerospace

engineering but has also found its way into bridge engineering (e.g., Xie and Xiang 1985, Wilde *et al.* 1996, Chen *et al.* 2000, Boonyapinyo *et al.* 2007, Mishra *et al.* 2007, Thang *et al.* 2008). The idea was first proposed in Roger (1977) and in the following form essentially in Abel (1979).

$$\mathbf{Q}(p) = \mathbf{A}_0 + \mathbf{A}_1 p + \mathbf{A}_2 p^2 + \sum_{l=1}^{n_L} \mathbf{A}_{l+2} \frac{p}{p + \gamma_l} \quad (11)$$

Compared to those in Eq. (7), the nominators of the rational summands in Eq. (11) additionally contain the complex reduced frequency p . This modification allows identifying the steady values $\mathbf{Q}(p=0)$ of the derivatives with the elements of the \mathbf{A}_0 matrix. The matching of the steady values is important for the evaluation of the divergence wind speed of the aeroelastic system in Section 5. When the constant parts of the rational summands in Eq. (11) are separated and combined with the \mathbf{A}_0 coefficient, Eq. (11) becomes for the single matrix elements of \mathbf{Q} equivalent to the formulation chosen before. Concerning the foregoing explanations it should be stressed that the equivalence of different time-domain approaches with convolution integrals and impulse responses can be easily shown in this way. Usually, constraints for $k \rightarrow \pm\infty$ are not included in the approximation procedure. Apart from Dirac impulses, the impulse responses in the time domain thus differ from the original values at $t = 0$. Without any further constraints, the coefficients \mathbf{A}_j , ($j > 0$) are determined by a least-squares fit after suitably placing the poles ($-\gamma_l$). Hence, the approximation procedure is often called Least-Squares Method. In an extended variant, the pole location on the negative real axis is repeatedly optimised by a nonlinear procedure whose results after each iteration step are used for a new least-squares fit of the \mathbf{A}_j coefficients. The following content of the article refers to this so-called Extended Least-Squares Method (Tiffany and Adams 1988). Through the use of identical poles for all elements of the derivative matrix, the size of the equation system for the aeroelastic system can be significantly reduced. A further size reduction without relevant loss of approximation quality can be achieved by using the more matrix-based (Extended) Minimum-State Method (Karpel 1981), which in other respects basically complies with the Extended Least-Squares Method.

As mentioned above, the approximation is done for discrete derivatives in an interval along the imaginary frequency axis. With $p = 0 + ik$ the real and imaginary part of the derivatives are

$$\operatorname{Re}(\mathbf{Q}(ik)) = \mathbf{A}_0 - \mathbf{A}_2 k^2 + \sum_{l=1}^{n_L} \mathbf{A}_{l+2} \frac{k^2}{k^2 + \gamma_l^2}, \quad \operatorname{Im}(\mathbf{Q}(ik)) = \mathbf{A}_1 k + \sum_{l=1}^{n_L} \mathbf{A}_{l+2} \frac{k \gamma_l}{k^2 + \gamma_l^2} \quad (12)$$

In Fig. 2, the behaviour of the summands is illustrated for a single derivative with the coefficients $A_i = 1$, ($i \neq 2$) and $A_2 = -1$. The curves of the rational summands are displayed for equally spaced pole locations ($-\gamma_l$) between (-0.1) and (-1.0). For the initial least-squares fit, the poles should be placed – concerning their absolute value - within the range of the absolute values of the imaginary frequencies at which the measured data is available (Tiffany and Adams 1988). The reason for this arrangement can be explained with Fig. 2 and Eq. (12) because the imaginary part of a rational summand with a pole at ($-\gamma_l$) has its extreme value above the imaginary axis at the reduced frequency $k = \pm\gamma_l$. Hence, the poles have their highest influence within the bandwidth of original values. The different suitability of rational functions for the approximation of derivatives of motion-

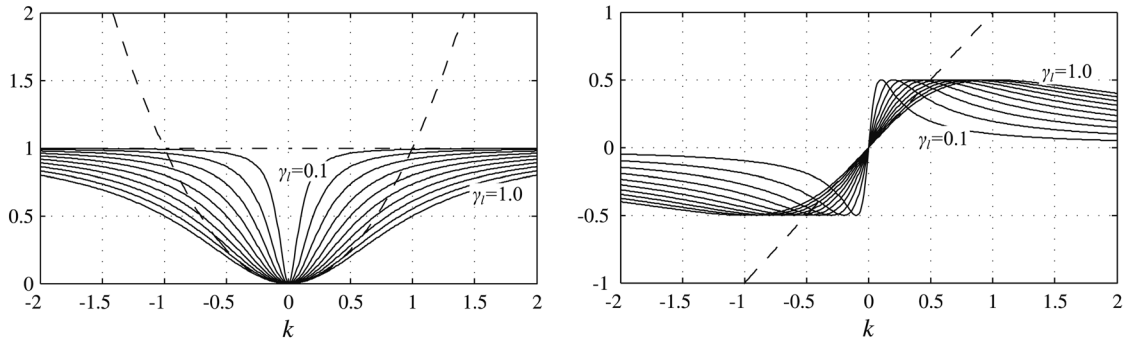


Fig. 2 Summands of the rational approximation of a derivative according to Eq. (12); real parts on the left, imaginary parts on the right

induced forces will be explained in the following section, mainly by means of two selected section shapes.

4. Approximation quality of rational functions

4.1 Motion-induced aerodynamic forces of the flat plate

The theoretical derivatives of the flat plate according to Theodorsen (1934) are determined for selected imaginary frequencies $k \in [0.1; 10]$ and are approximated with Eq. (11) pursuant to the Extended Least-Squares Method. Steady values are incorporated in the \mathbf{A}_0 matrix. Contrary to the recommendation given in the previous section, the initial positions of the poles are selected within the interval $[-1.0; 0]$ as will be justified later on.

The approximation results are as follows: Nearly independent of the number of lag terms n_L , the coefficients of the polynomial summands almost exactly include the non-circulatory aerodynamic forces and parts of the circulatory ones. A polynomial part of degree two is thus justified for approximating the theoretical flat plate derivatives. The rational summands contain the remaining parts of the circulatory forces. For the flat plate, the particular suitability of the lag terms with negative real poles can be qualitatively explained in the time domain. The decaying exponential functions describe the effect of drifting vortices arising at the leeward edge and their girder-bound counterpart.

In Fig. 3, the theoretical derivatives and their rational approximations with $n_L = 5$ are exemplarily illustrated for the derivative Q_{11} against reduced frequencies of the imaginary axis. Their behaviour along the negative part of the axis follows from their complex-conjugate properties. Along this axis, the extremely good approximation is evident.

A surface plot of the Q_{11} real part over an area of the complex frequency plane is displayed in Fig. 4. The poles are visible in the interval $[-1.0; 0]$ of the negative real frequency axis. For the flat plate, derivatives can also be theoretically evaluated for complex frequencies based on the generalised Theodorsen function (Edwards 1977). In Fig. 5, the difference between the theoretically exact values and the rationally approximated ones is shown for the real part of the already mentioned derivative. Since the theoretical values are not defined for frequencies on the negative

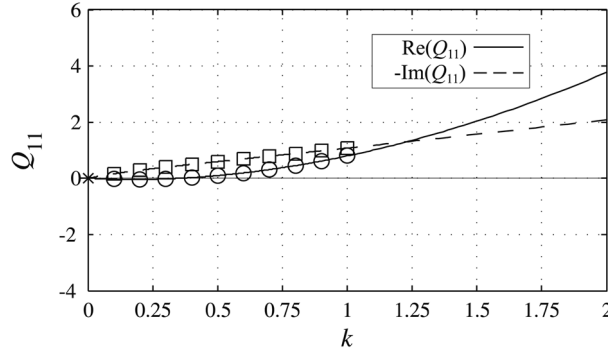


Fig. 3 Derivative Q_{11} of a flat plate along the imaginary axis of the complex frequency plane. The original, theoretical values are displayed with markers, the rational approximations with lines

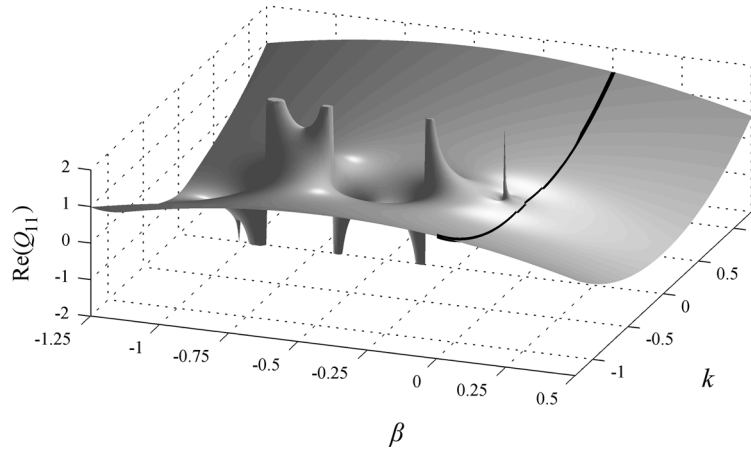


Fig. 4 Real part of the flat plate's derivative Q_{11} above the complex frequency plane. The approximation along the imaginary frequency axis is graphically accentuated. Absolute values are limited by the displayed maximum values of the vertical axis

real axis and at the origin, the difference is not displayed. Even if the poles have other initial positions in a larger interval, the nonlinear optimisation places them in the complex frequency interval $[-2.0; 0]$. The imaginary part of the generalised Theodorsen function features a perceptible discontinuity within this interval. The result of the location optimisation is thus predictable and it is justified to initially place the poles within the smaller interval. In the left half-plane, the difference between the original values and their approximation vanishes for complex frequencies with high absolute values. In the right half-plane almost no differences are visible. The strip-like area $|\beta| < 0.15$ in the left frequency half-plane is important for the aeroelastic system because the eigenvalues especially in this low-damped area is closely connected to the quality of its dynamic behaviour. Hence, a good approximation of the fluid force is necessary there. Perceptible deviations only exist near the pole with the smallest absolute value. Imaginary parts of the reduced frequency of bridges that are interfered by this pole are not to be expected. Apart from this small area, the approximation within the strip can be judged as excellent on the basis of this figure.

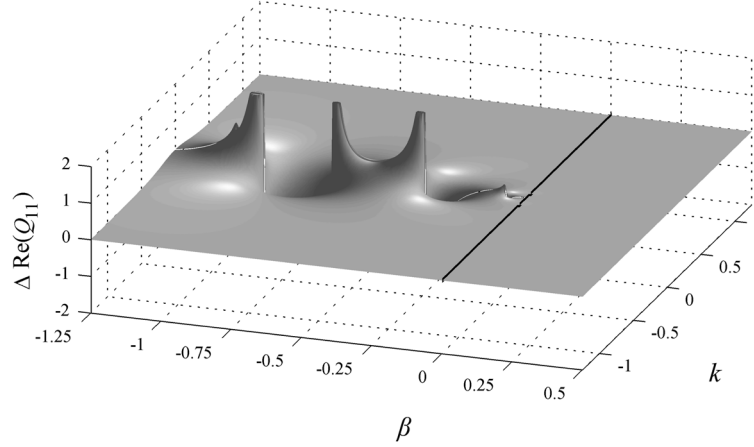


Fig. 5 Difference between the real part of the flat plate's derivative Q_{11} and its rational approximation above the complex frequency plane. Absolute values are limited by the displayed maximum values of the vertical axis

4.2 Motion-induced aerodynamic forces of real bridge cross sections

The unsteady frequency-domain approach, which is based on a linear dependence of forces on displacements, is problematic for bluff and sharp-edged cross sections, as they are often applied for real bridge girders. In contrast to the theoretically described flat plate, the forces also depend on the mean angle of attack. These difficulties are not discussed herein.

The derivatives for real bridge cross sections cannot be analytically calculated with the potential theory. As mentioned above, they are usually experimentally determined for imaginary frequencies in a wind or a water tunnel with a scaled section model. Additionally, numerical, CFD-based procedures have been established in recent years to achieve comparable results (e.g., Larsen and Walther 1998, Chen *et al.* 2002, Starossek *et al.* 2009). In this article, experimentally determined derivatives of idealised cross sections according to Bergmann (2004) are used. The selected cross sections are shown in Fig. 6. Bergmann's results are also used in Starossek *et al.* (2009).

Measured derivatives are extracted for most cross sections in intervals $k \in [0.1; 1.05]$ as they are relevant for bridges. Once again, the rational function approximation procedure is carried out with the Extended Least-Squares Method. Initial positions of the poles are defined as explained in Section 3 and the steady values of the derivatives are again incorporated into the \mathbf{A}_0 matrix.

Table 1 and Table 2 list the approximation results in a simplified way. The used total approximation error J is defined according to Tiffany and Adams (1988).

$$J = \sqrt{\sum_{j,l,\lambda} |Q_{jl}^{appr}(ik_\lambda) - Q_{jl}(ik_\lambda)|^2 / \max_{n_k}(1, |Q_{jl}(ik_\lambda)|^2)} \quad (13)$$

In this definition Q_{jl} stands for the original value which is given for n_k discrete reduced frequencies ik_λ , and Q_{jl}^{appr} is the approximation.

The Tacoma bridge cross section can be exemplarily used to explain problems that occur when derivatives of real bridge sections are approximated with rational functions. Contrary to the moved

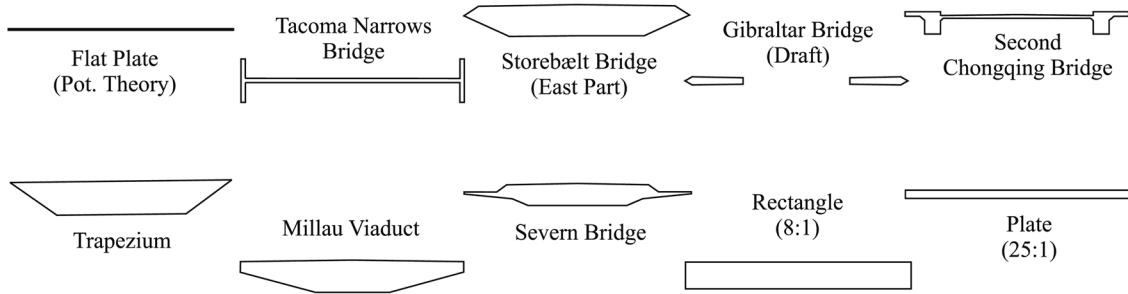


Fig. 6 Cross section shapes addressed in this article. Measured derivatives according to Bergmann (2004)

Table 1 Averaged absolute values of the coefficients of the rational approximation. The upper and lower values correspond to the coefficients of the polynomial and rational summands, respectively

| n_L | Flat Plate (Pot. Theory) | First Tacoma Narrows Bridge | Storebælt Bridge (East Part) | Gibraltar Bridge (Draft) | Second Chongqing Bridge |
|-------|-----------------------------|--------------------------------|---------------------------------|-----------------------------|----------------------------|
| 3 | 0.6146 | 2.480 | 0.4555 | 0.3413 | 3.037 |
| | 0.1557 | 5.305 | 0.3983 | 0.5780 | 109.4 |
| 5 | 0.6146 | 5.593 | 0.5304 | 0.3363 | 2.175 |
| | 0.2625 | 237.8 | 7.078 | 0.9102 | 104.3 |
| 7 | 0.6146 | 8.827 | 0.5031 | 0.2623 | 0.9595 |
| | 3.878 | 6457 | 170.8 | 254.2 | 1150 |
| n_L | Trapezium | Millau Viaduct | Severn Bridge | Rectangle (8:1) | Plate (25:1) |
| 3 | 0.5224 | 0.5513 | 0.5326 | 0.7108 | 0.6210 |
| | 0.4811 | 0.2171 | 0.3449 | 0.7934 | 0.3407 |
| 5 | 0.5220 | 0.5989 | 0.5613 | 0.7815 | 0.6978 |
| | 2.369 | 0.9331 | 0.7919 | 4.785 | 12.13 |
| 7 | 0.6253 | 0.7378 | 0.6217 | 1.001 | 0.9241 |
| | 351.7 | 184.6 | 226.8 | 911.9 | 349.4 |

flat plate, there are also more or less distinct vortices arising from the windward part of a bluff and sharp-edged profile. Especially in the case of the Tacoma bridge cross section, these vortices decisively affect the flow around the bridge deck (e.g., Larsen 2000). Its derivatives clearly differ from those of the flat plate.

First of all, as shown in Fig. 7, there is a qualitatively acceptable approximation above the imaginary axis. Unlike the flat plate case, the frequency range of the poles is not essentially changed by the nonlinear optimisation of their location. The rational functions rather approximate the derivatives by a strong weighting of the rational summands. For increasing absolute pole values, the coefficients of the rational summands of Eq. (11) appear with changing signs. Thus, the sum of the rational summands results in the desired behaviour along parts of the imaginary axis. Fig. 8 displays the real part of the Q_{11} derivative over an area of the complex frequency plane. In contrast

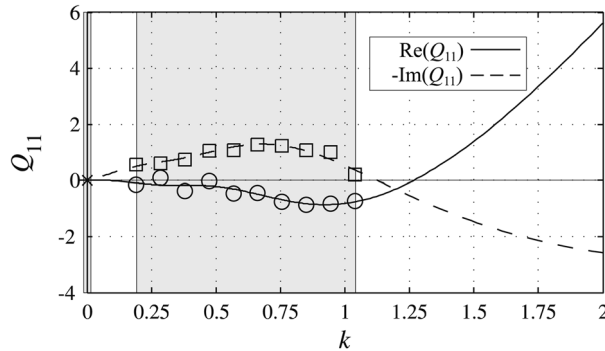


Fig. 7 Derivative Q_{11} of the Tacoma bridge cross section along the imaginary axis of the complex frequency plane. The original, theoretical values are displayed with markers, the rational approximations with lines

to the corresponding Fig. 4 of the flat plate, the pole-influenced areas, where the approximation functions are strongly distorted, are widely extended. When comparing the averaged absolute values of coefficients of the rational summands in the upper fields of the first two columns in Table 1, this effect becomes apparent as well. It must be pointed out that the values should only be considered in their order of magnitude because the derivatives are determined for different cross sections and different pole locations. As can be seen in Table 1, the mentioned values also increase when more lag terms are used, that is when the approximation tends towards an interpolation. This can also be observed for the flat plate described by the potential theory. When comparing the coefficients of the rational summands of all cross sections, it can be found that, especially for sections with large vortices arising from the windward side, the approximation is performed with highly weighted lag terms.

Off the imaginary axis, the dominance of the rational summands leads to a strongly distorted behaviour of the approximation. Since the derivatives of real bridge sections are normally not

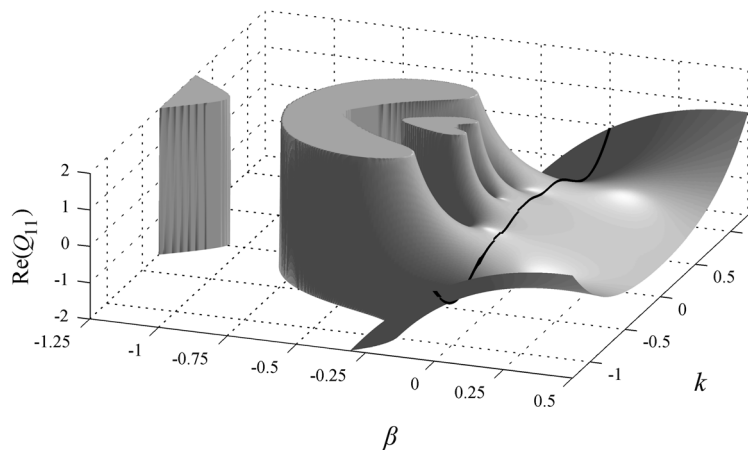


Fig. 8 Real part of the derivative Q_{11} of the Tacoma bridge cross section above the complex frequency plane. The approximation along the imaginary frequency axis is graphically accentuated. Absolute values are limited by the displayed maximum values of the vertical axis

Table 2 Total approximation error $J \cdot 10^4$ according to Eq. (13) divided by the number n_k of frequencies where derivatives are measured

| n_L | Flat Plate (Pot. Theory) | First Tacoma Narrows Bridge | Storebælt Bridge (East Part) | Gibraltar Bridge (Draft) | Second Chongqing Bridge |
|-------|-----------------------------|--------------------------------|---------------------------------|-----------------------------|----------------------------|
| 3 | 0.4632 | 1039 | 147.3 | 20.36 | 236.3 |
| 5 | 0.1754 | 857.5 | 134.4 | 15.33 | 171.5 |
| 7 | 0.2170 | 813.7 | 129.0 | 29.97 | 142.5 |
| n_L | Trapezium | Millau Viaduct | Severn Bridge | Rectangle (8:1) | Plate (25:1) |
| 3 | 91.30 | 42.36 | 47.87 | 104.6 | 42.84 |
| 5 | 87.39 | 25.24 | 33.45 | 73.84 | 36.80 |
| 7 | 85.70 | 27.09 | 33.34 | 81.88 | 20.58 |

determined for true complex frequencies with non-zero real parts, they are not available for reference. Nevertheless, it can be stated that aerodynamic forces are expressed in an absolutely wrong manner within the already mentioned area $|\beta| < 0.15$ if the coefficients of the lag terms are too large. Conclusions concerning the quality of the dynamic system based on these distorted descriptions of fluid forces are expected to significantly differ from reality.

Increasing the number of lag terms is not associated with continuously reducing the approximation error (Table 2). As can be shown with results not presented here, this effect is only local. In principle, a higher number of rational summands leads to a better approximation of the derivatives above the imaginary axis, normally accompanied by a larger distortion in the adjacent frequency regions on the imaginary axis and the complex plane. The coefficients of the polynomial are not independent of the number of lag terms but their absolute values remain in the same order of magnitude (Table 1). Problems caused by these coefficients are addressed in Section 5.

5. Approximation effects on the aeroelastic system

5.1 Modelling and investigating the aeroelastic system

The time-domain representation of the motion-induced forces results in general when applying the convolution theorem of the Laplace transform to Eq. (6)

$$\mathbf{f}(\bar{t}) = \mathbf{G}(\bar{t})^{\bar{t}} * \xi_s(\bar{t}) = \int_0^{\bar{t}} \mathbf{G}(\bar{t} - \bar{\tau}) \cdot \xi_s(\bar{\tau}) d\bar{\tau} \quad (14)$$

It is commonly known that it is also possible to use equivalent formulas with step responses or similar expressions instead of the impulse response $\mathbf{G}(t)$. The integrals must be evaluated for each time step. The numerical effort to solve this equation is hence rather high. Especially when the coefficients of the rational summands of Eq. (11) have high values, the time axis around $\bar{\tau} \approx \bar{t}$ must be discretised in very small steps to take very strong variations of the impulse response into account.

If the transfer function is described with rational functions there is a major advantage. The rational summands can be transformed into linear differential equations with constant coefficients after introducing artificial aerodynamic states $\xi_{a,l}$, which are also called lag states.

$$\xi_a = (\xi_{a,1}^T \dots \xi_{a,n_L}^T)^T \quad (15)$$

$$\xi_{a,l} = \mathbf{A}_{l+2} \frac{p}{p + \gamma_l} \xi_s \quad \bullet \text{---} \circ \quad \bar{\mathbf{D}} \xi_{a,l} = -\gamma_l \xi_{a,l} + \mathbf{A}_{l+2} \bar{\mathbf{D}} \xi_s \quad (16)$$

Usually, for investigations of the dynamic behaviour, the bridge structure can also be appropriately described by linear differential equations with constant coefficients. If necessary, the structural stiffness has to be linearised. Thus, the aeroelastic system can be represented by a linear, time-invariant state-space model.

$$\mathbf{D}\mathbf{x}(t) = \mathbf{A}\mathbf{x}(t), \quad \mathbf{x}(t) = (\xi_s^T \mathbf{D} \xi_s^T \xi_a^T)^T \quad (17)$$

The elements of the system matrix \mathbf{A} can, for instance, be taken from Tiffany and Adams (1988). The mean horizontal wind speed U occurs in the system matrix \mathbf{A} as a parameter. There are two reasons. The factor q_0 contains U (cp. Eq. 3) and the generalised differentiation \mathbf{D} with respect to the absolute time t has to be used. The coefficients \mathbf{A}_0 , \mathbf{A}_1 and \mathbf{A}_2 are incorporated in the stiffness, damping and mass of the aeroelastic system, respectively. Hence, these expressions can be regarded as parts of the corresponding properties of the air flow around the structure. In addition to the structural degrees of freedom ξ_s , the state vector \mathbf{x} contains the vector ξ_a of the artificial aerodynamic states $\xi_{a,l}$. When taking into account gusts and other loads, the state-space equation can be extended with an input term. Together with an output equation, a full state-space model is thus available.

The dynamic characteristics of the aeroelastic system can be evaluated with an eigenvalue analysis of the system matrix \mathbf{A} . System stability is of major interest in this context. Due to the effect of motion-induced aerodynamic forces, aeroelastic instabilities can occur in the form of flutter and divergence. Unless otherwise explained, the two terms should specifically denote the cases of neutral stability. Since the system matrix contains the mean horizontal wind speed U , a parameter-dependent linear eigenvalue problem must be solved.

The two-dimensional, generalised system in Fig. 1 is used as an example with the characteristic structural properties given in Table 3. Concerning the aerodynamic behaviour, both the rational approximations of the flat plate described with the potential theory and the Tacoma bridge cross section are considered.

Table 3 Structural properties of the two-dimensional bridge model

| | |
|---------------------------------|----------------------------------------------------------------------|
| half deck width: | $b = 15.0 \text{ m}$ |
| mass: | $m = 25.0 \cdot 10^3 \text{ kg/m}$ |
| moment of inertia: | $I = 2.80 \cdot 10^6 \text{ kgm}^2/\text{m}$ |
| eigenfrequencies: | $\omega_h = 0.628 \text{ 1/s}$ $\omega_\alpha = 1.76 \text{ 1/s}$ |
| logarithmic damping decrements: | $\delta_h = 0.0126$ $\delta_\alpha = 0.0126$ |

5.2 Eigenvalues for the flat-plate cross section

For the flat plate, neutral stability appears at the zero crossings of the eigenvalue real part curves (Fig. 9) as flutter at $U = 82.8$ m/s and as divergence at $U = 99.1$ m/s. This identification is possible when inspecting the eigenvalues and state eigenvectors. The indifferent flutter point occurs in two complex-conjugate eigenvectors with complex elements. Its eigenfrequencies are purely imaginary and complex conjugate (Fig. 10). In the case of the flat plate, both structural degrees of freedom appear in the same order of magnitude, as can be predicted for the classical bending-torsional flutter. Indifferent divergence has only one eigenvector, the element values of which are real and vanish in the velocities Dx and the lag states ξ_a . Its eigenfrequency is zero.

The eigenvalues close to the negative real axis originate in the lag terms of the rational approximation of the derivatives. This can be observed when using the reduced frequency plane, as it is done in Fig. 10. For a system characterisation, the eigenvalues with small absolute values of the real parts are important. They are all located within areas of a good derivative approximation.

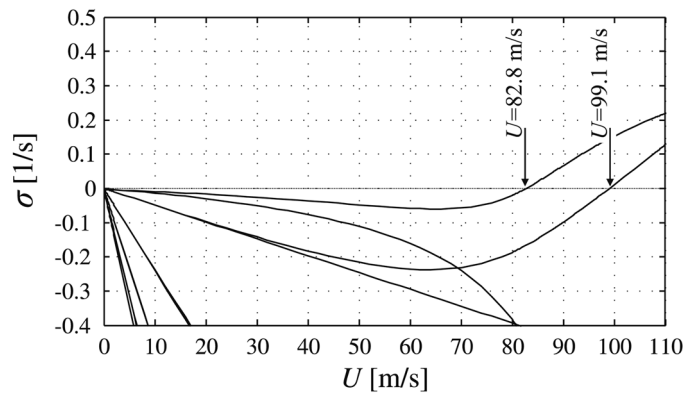


Fig. 9 Real parts of the eigenvalues of an aeroelastic system with the flat plate cross section

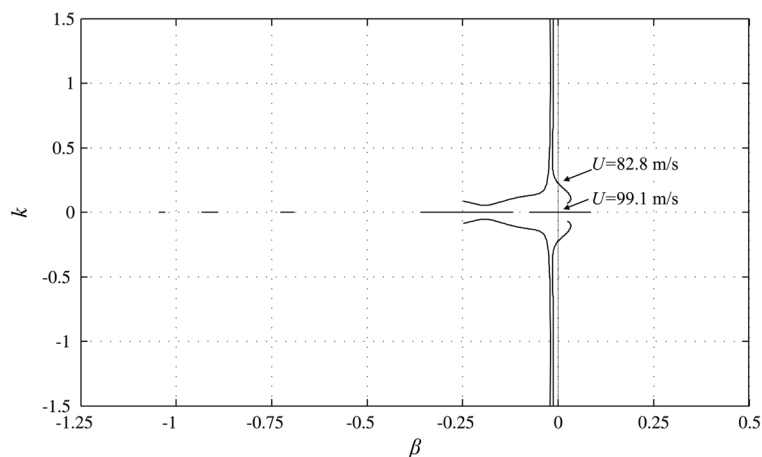


Fig. 10 Eigenvalues of an aeroelastic system with the flat plate cross section displayed in the reduced complex frequency plane

5.2 Eigenvalues for the Tacoma bridge cross section

For the Tacoma bridge cross section, an indifferent flutter point with a dominant torsional part can be identified at $U = 29.9$ m/s when considering Fig. 12 and the associated eigenvector. Almost pure torsional flutter is typical of this section shape.

The instable range between $U = 0.6$ m/s and $U = 8.1$ m/s in Fig. 11 does not exist in reality. It is caused by the rational function approximation. The coefficients of the polynomial terms, which have already been mentioned in Section 4, cannot be interpreted as has been done for the flat plate case. The \mathbf{A}_0 matrix corresponds to the stiffness that is generated by the air flow around the structure and is derived from the steady values of the aerodynamic forces within this article. Its elements are hence well-founded. The elements of the \mathbf{A}_2 matrix can be interpreted as part of the mass of the fluid flow but they are negligible in comparison with the much larger mass of the structure. More problems are caused by the \mathbf{A}_1 matrix. It is responsible for the behaviour of the imaginary parts of the derivatives at high reduced frequencies, as can be seen in Eq. (12) and in Fig. 2. As is generally known, the imaginary parts of the derivative elements on the main diagonal can, for positive reduced frequencies on the imaginary axis, be regarded as a negative damping, generated by the air flow. In the case of the Tacoma bridge cross section, such positive values of the Q_{22} element are responsible for the torsional flutter. As can be observed from Fig. 7, a positive \mathbf{A}_1 coefficient causes these unfavourable values for the Q_{11} element as well, but in this case outside the identification interval. When comparing Figs. 7, 11 and 12 it can be discovered that the low, instable speed range is provoked by this poor shape of the approximation outside the grey-coloured identification range. Thus, this effect must always be anticipated if positive elements occur on the main diagonal of the \mathbf{A}_1 matrix. Further calculations show that the \mathbf{A}_1 effect appears even for streamlined sections whose aerodynamic behaviour is similar to that of the flat plate.

Unlike the flat plate case, the pole influenced, distorted behaviour of the motion-induced forces generates numerous eigenvalues in the left frequency half-plane off the real axis (Fig. 12). As a consequence of the low approximation quality of rational functions for the Tacoma bridge cross section, all results in Fig. 12 that are located outside the grey-coloured areas are questionable from a physical point of view.

In the case of controlled aeroelastic systems, as they have been addressed in the introduction of this article, the effects of the rational function approximation must also be kept in mind. For

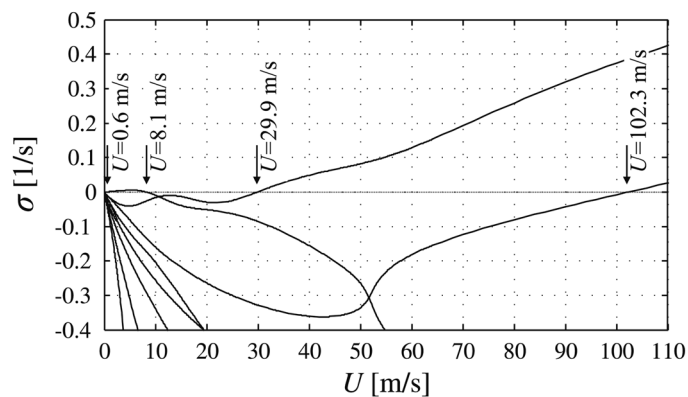


Fig. 11 Real parts of the eigenvalues of an aeroelastic system with the Tacoma bridge cross section

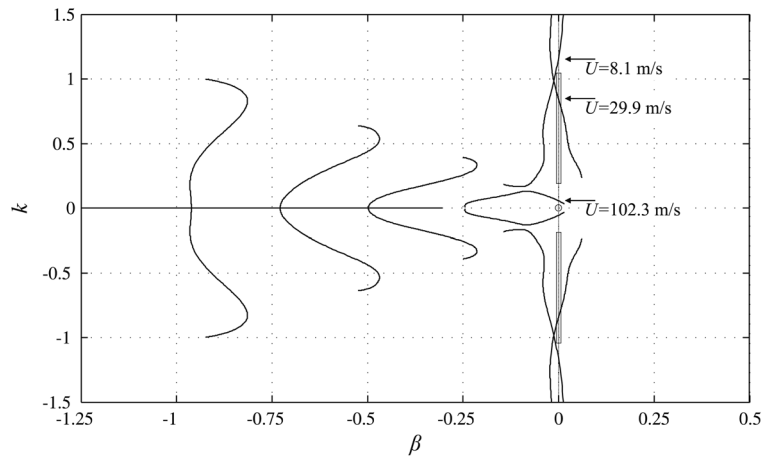


Fig. 12 Eigenvalues of an aeroelastic system with the Tacoma bridge cross section displayed in the reduced complex frequency plane

instance, single eigenvalues with undesired characteristics like uncontrollability, which are caused by the poor approximation quality of rational function for motion induced aerodynamic forces, can occur especially along the negative real axis. These problems are described in Kirch *et al.* (2009a,b).

6. Conclusions

The description of the transfer behaviour of motion-induced aerodynamic forces with rational functions has been explained in a general way. The suitability of complex-conjugate and multiple poles for non-streamlined bridge sections still requires systematic investigation. For the well-known case of simple, real poles, the approximation of derivatives of motion-induced wind forces has been performed using the Extended Least-Squares Method. It has been shown that this approximation only yields convincing results off the identification interval for either the flat plate described by the potential theory or for sections with a similar air flow around them. The quality of the approximation of aerodynamic forces significantly affects the quality of the model of the aeroelastic system. Additionally, positive elements at the main diagonal of the \mathbf{A}_1 approximation matrix lead to unrealistic, unstable states of the aeroelastic system within the range of small mean wind speeds.

Acknowledgements

We gratefully acknowledge the support given to this work by the International Graduate College IGC 802 of the German Research Foundation (DFG).

References

Abel, I. (1979), "An analytical technique for predicting the characteristics of a flexible wing equipped with an

- active flutter-suppression system and comparison with wind-tunnel data”, NASA-TP-1367, Technical Paper, NASA.
- Bergmann, D. (2004), “Experimentelle Ermittlung der instationären aerodynamischen Eigenschaften von Brückenprofilen im Wasserkanal”, Dissertation, Universität Stuttgart, Germany (in German).
- Boonyapinyo, V., Aksorn, A. and Lukkunaprasit, P. (2007), “Suppression of aerodynamic response of suspension bridges during erection and after completion by using tuned mass dampers”, *Wind Struct.*, **10**(1), 1-22.
- Botez, R.M., Dinu, A.D., Cotoi, I., Stathopoulos, N., Therien, S., Dickinson, M. and Rathé, A. (2007), “Improved method for creating time-domain unsteady aerodynamic models”, *J. Aircraft*, **20**(3), 204-208.
- Chen, A., He, X. and Xiang, H. (2002), “Identification of 18 flutter derivatives of bridge decks”, *J. Wind Eng. Ind. Aerod.*, **90**(12-15), 2007-2022.
- Chen, X., Matsumoto, M. and Kareem, A. (2000), “Time domain flutter and buffeting response analysis of bridges”, *J. Eng. Mech- ASCE*, **126**(1), 7-16.
- Edwards, J.W. (1977), “Unsteady aerodynamic modeling and active aeroelastic control”, NASA-CR-148019, Contractor Report, NASA.
- Eversman, W. and Tewari, A. (1991), “Consistent rational-function approximation for unsteady aerodynamics”, *J. Aircraft*, **28**(9), 545-552.
- Garrick, I.E. (1938), “On some reciprocal relations in the theory of nonstationary flows”, NACA-TR-629, Technical Report, NACA.
- Jones, R.T. (1938), “Operational treatment of the nonuniform-lift theory in airplane dynamics”, NACA-TN-667, Technical Note, NACA.
- Karpel, M. (1981), “Design for active and passive flutter suppression and gust alleviation”, NASA-CR-3482, Contractor Report, NASA.
- Kirch, A. and Peil, U. (2009), “Fundamental restrictions for the closed-loop control of wind-loaded, slender bridges”, *Wind Struct.*, **12**(5), 457-474.
- Kirch, A., Peil, U. and Borri, C. (2009a), “Limits for the control of wind-loaded slender bridges with movable flaps; Part I: Aerodynamic modelling, state-space model and open-loop characteristics of the aeroelastic system”, *Proceedings of the 5th European and African Conference on Wind Engineering EACWE5*, Florence, Italy.
- Kirch, A., Peil, U. and Borri, C. (2009b), “Limits for the control of wind-loaded slender bridges with movable flaps; Part II: Controller design, closed-loop characteristics of the aeroelastic system and gust alleviation”, *Proceedings of the 5th European and African Conference on Wind Engineering EACWE 5*, Florence, Italy.
- Klöppel, K. and Thiele, F. (1967), “Modellversuche im Windkanal zur Bemessung von Brücken gegen die Gefahr winderregter Schwingungen”, *Der Stahlbau*, **36**, 353-365 (in German).
- Küssner, H.G. (1936), “Zusammenfassender Bericht über den instationären Auftrieb von Flügeln”, *Luftfahrtforschung*, **13**, 410-424 (in German).
- Küssner, H.G. and Schwarz, L. (1940), “Der schwingende Flügel mit aerodynamisch ausgeglichenem Ruder”, *Luftfahrtforschung*, **17**, 337-354 (in German).
- Larsen, A. and Walther, J.H. (1998), “Discrete vortex simulation of flow around five generic bridge deck sections”, *J. Wind Eng. Ind. Aerod.*, **77-78**, 591-602.
- Larsen, A. (2000), “Aerodynamics of the Tacoma Narrows Bridge — 60 years later”, *Eng. Struct.*, **10**(4), 243-248.
- Lin, Y., Cheng, C. and Lee, C. (1999), “Multiple tuned mass dampers for controlling coupled buffeting and flutter of long-span bridges”, *Wind Struct.*, **2**(4), 267-284.
- Mishra, S.S., Kumar, K. and Krishna, P. (2007), “A study of wind effect on damping and frequency of a long span cable-stayed bridge from rational function approximation of self-excited forces”, *Wind Struct.*, **10**(3), 215-232.
- Omenzetter, P., Wilde, K. and Fujino, Y. (2000), “Suppression of wind-induced instabilities of a long span bridge by a passive deck-flaps control system; Part I: Formulation”, *J. Wind Eng. Ind. Aerod.*, **87**, 61-79.
- Pourzeynali, S. and Datta, T.K. (2002), “Control of flutter of suspension bridge deck using TMD”, *Wind Struct.*, **5**(5), 407-422.
- Roger, K. (1977), “Airplane math modelling methods for active control design”, *Structural Aspects of Active Controls – AGARD-CP-228*, 4-1 – 4-11.

- Simiu, E. and Scanlan, R.H. (1996), *Wind Effects on Structures: Fundamentals and Applications to Design*, 3th Editoin., Wiley, New York.
- Stark, V.J.E. (1984), "General Equations of motion for an elastic wing and method of solution", *AIAA J.*, **22**(8), 1146-1153.
- Starossek, U., Aslan, H. and Thiesemann, L. (2009), "Experimental and numerical identification of flutter derivatives for nine bridge deck sections", *Wind Struct.*, **12**(6), 519-540.
- Sternberg, A. (1991), "Stability investigations of long-span bridges using indicial functions with oscillatory terms", *Probabil. Eng. Mech.*, **6**(3-4), 164-174.
- Thang, N.D., Katsuchi, H., Yamada, H. and Sasaki, E. (2008), "Study on effect of accuracy in rational function approximation for self-excited forces of a long-span bridge", *Proceedings of the 4th International Conference on Advances in Wind and Structures*, Jeju , Korea.
- Theodorsen, T. (1934), "General theory of aerodynamic instability and the mechanism of flutter", NACA TR-496, Technical Report, NACA.
- Theodorsen, T. and Garrick, I.E. (1941), "Nonstationary flow about a wing-aileron-tab combination including aerodynamic balance", NACA-TR-736, Technical Report, NACA.
- Tiffany Hoadley, S. and Adams, Jr., W.M. (1988), "Nonlinear programming extensions to rational function approximation methods for unsteady aerodynamic forces", NASA-TP-2776, Technical Paper, NASA.
- Wilde, K., Fujino, Y. and Masukawa, J. (1996), "Time domain modelling of bridge deck flutter", *Earthq. Eng. Struct. D.*, **13**, 93-104.
- Xie, J.M. and Xiang, H.F. (1985), "State-space method for 3-D flutter analysis of bridge structures", *Proceedings of the First Asia Pacific Symposium on Wind Engineering*, Roorkee , India.

CC

Appendix

The following notation is used in this article. Table 3 defines additional variables.

| | |
|------------------|---------------------------------------------------------------------------------------------------------------------|
| h, α | aerodynamically effective structural degrees of freedom of the example system (Fig. 1) |
| L, M | motion-induced aerodynamic vertical force and moment acting on the example system (Fig. 1) |
| U | horizontal mean wind speed |
| ρ | air density ($\approx 1.25 \text{ kg/m}^3$) |
| b, B | half width and total width of the aerodynamically effective cross section |
| H_j^*, A_j^* | aerodynamic derivatives according to Simiu and Scanlan (1996) |
| K | reduced frequency related to B |
| \mathbf{f} | vector of motion-induced aerodynamic forces |
| $\mathbf{Q}(p)$ | matrix of aerodynamic derivatives |
| $Q(p)$ | element of the \mathbf{Q} matrix |
| ξ_s | vector of aerodynamically effective structural degrees of freedom |
| q_0 | factor in the aerodynamic transfer equation |
| s | complex frequency |
| σ, ω | real and imaginary part of the complex frequency |
| p | reduced complex frequency related to b |
| β, k | real and imaginary part of the reduced complex frequency related to b |
| $\mathbf{G}(s)$ | matrix of the aerodynamic transfer function or aerodynamic admittance function of motion-induced aerodynamic forces |

| | |
|--------------------------------------------------|-----------------------------------------------------------------------------------------------------------------------|
| $A_j, A_{\mu\kappa}$ | coefficients of the rational function approximation |
| γ | negative value of a pole of the derivative approximation |
| ν | order or multiplicity of the pole of the derivative approximation |
| n | total number of poles of the derivative approximation |
| t, \bar{t} | time and non-dimensionalised time |
| $\mathbf{G}(t)$ | matrix of impulse responses |
| G | element of the $\mathbf{G}(t)$ matrix |
| $Q(\bar{t})$ | time-domain analogon of the derivative $Q(p)$ |
| \mathbf{A}_j | coefficient matrix of the rational function approximation |
| n_L | number of lag terms in the rational function approximation |
| J | approximation error |
| Q_{jl}, Q_{jl}^{appr} | derivative and approximated derivative if both ones appear in an equation |
| n_k | number of frequencies, where derivatives are measured |
| $\tau, \bar{\tau}$ | time and non-dimensionalised time within an integral |
| $\xi_{as}, \xi_{a,j}$ | vector and subvector of aerodynamic states |
| \mathbf{x} | state vector of the state-space model |
| \mathbf{A} | system matrix of the state-space model |
| $j, l, \kappa, \lambda, \mu$ | matrix and vector indices |
| Δ | difference |
| $(\dot{})$ | differentiation with respect to the time t |
| D, \bar{D} | generalised differentiation (i.e., using distributions) with respect to the time t and the non-dimensionalised time |
| $\delta, \bar{\delta}$ | Dirac impulse with respect to the time t and the non-dimensionalised time \bar{t} |
| $()^T$ | transposition |
| $()^c$ | complex conjugate |
| i | imaginary unit; $i^2 = -1$ |
| $ $ | absolute value |
| φ | argument of a complex value |
| $\text{Re}(), \text{Im}()$ | real and imaginary part of a complex value |
| $\bullet \text{---} \circ$ | symbol for corresponding variables, equations, etc. in frequency and time domain |
| $\overset{t}{*}, \overset{\bar{t}}{*}$ | symbols for convolution with respect to the time t and the non-dimensionalised time \bar{t} |